

















## Topography Controls Variability in Circumpolar Permafrost Thaw Pond Expansion

### Key Points:

- Decadal-scale thermokarst pool expansion was observed at 12 (plus or minus 4) of 27 landscapes monitored throughout the Arctic
- Expanding thermokarst pools were most likely to be found in topographically convex positions within hilly landscapes
- Trends in air temperature alone were a poor predictor of recent thermokarst pool expansion

C. J. Abolt<sup>1</sup> , A. L. Atchley<sup>1</sup> , D. R. Harp<sup>1,2</sup> , M. T. Jorgenson<sup>3</sup> , C. Witharana<sup>4</sup> ,  
W. R. Bolton<sup>5</sup> , J. Schwenk<sup>1</sup> , T. Rettelbach<sup>6,7</sup> , G. Grosse<sup>6,7</sup> , J. Boike<sup>6,8</sup> , I. Nitzke<sup>6</sup> ,  
A. K. Liljedahl<sup>9</sup> , C. T. Rumpca<sup>10</sup>, C. J. Wilson<sup>1</sup> , and K. E. Bennett<sup>1</sup> 

<sup>1</sup>Earth and Environmental Sciences Division, Los Alamos National Laboratory, Los Alamos, NM, USA, <sup>2</sup>Now at: Science and Analytics Team, The Freshwater Trust, Portland, OR, USA, <sup>3</sup>Alaska Ecoscience, Fairbanks, AK, USA, <sup>4</sup>Department of Natural Resources and the Environment, University of Connecticut, Storrs, CT, USA, <sup>5</sup>Environmental Sciences Division, Oak Ridge National Laboratory, Oak Ridge, TN, USA, <sup>6</sup>Alfred Wegener Institute Helmholtz Centre for Polar and Marine Research, Potsdam, Germany, <sup>7</sup>Institute of Geosciences, University of Potsdam, Potsdam, Germany, <sup>8</sup>Department of Geography, Humboldt-Universität zu Berlin, Berlin, Germany, <sup>9</sup>Woodwell Climate Research Center, Falmouth, MA, USA, <sup>10</sup>Beacom College of Computer and Cyber Sciences, Dakota State University, Madison, SD, USA

### Supporting Information:

Supporting Information may be found in the online version of this article.

### Correspondence to:

C. J. Abolt,  
[chuck.abolt@utexas.edu](mailto:chuck.abolt@utexas.edu)

### Citation:

Abolt, C. J., Atchley, A. L., Harp, D. R., Jorgenson, M. T., Witharana, C., Bolton, W. R., et al. (2024). Topography controls variability in circumpolar permafrost thaw pond expansion. *Journal of Geophysical Research: Earth Surface*, 129, e2024JF007675. <https://doi.org/10.1029/2024JF007675>

Received 1 FEB 2024

Accepted 3 SEP 2024

**Abstract** One of the most conspicuous signals of climate change in high-latitude tundra is the expansion of ice wedge thermokarst pools. These small but abundant water features form rapidly in depressions caused by the melting of ice wedges (i.e., meter-scale bodies of ice embedded within the top of the permafrost). Pool expansion impacts subsequent thaw rates through a series of complex positive and negative feedbacks which play out over timescales of decades and may accelerate carbon release from the underlying sediments. Although many local observations of ice wedge thermokarst pool expansion have been documented, analyses at continental to pan-Arctic scales have been rare, hindering efforts to project how strongly this process may impact the global carbon cycle. Here we present one of the most geographically extensive and temporally dense records yet compiled of recent pool expansion, in which changes to pool area from 2008 to 2020 were quantified through satellite-image analysis at 27 survey areas (measuring 10–35 km<sup>2</sup> each, or 400 km<sup>2</sup> in total) dispersed throughout the circumpolar tundra. The results revealed instances of rapid expansion at 44% ( $\pm 15\%$ ) of survey areas. Considered alone, the extent of departures from historical mean air temperatures did not account for between site variation in rates of change to pool area. Pool growth was most clearly associated with upland (i.e., hilly) terrain and elevated silt content at soil depths greater than one meter. These findings suggest that, at short time scales, pedologic and geomorphologic conditions may exert greater control on pool dynamics in the warming Arctic than spatial variability in the rate of air temperature increases.

**Plain Language Summary** Ice wedge thermokarst pools are meter-scale water features with a distinctive shape that form on the tundra in response to permafrost thaw. They occupy pits in the ground surface caused by the melting of ice wedges, or subsurface ice bodies which form an interconnected network that manifests at the surface as polygonal ground. Ice wedge thermokarst pool growth not only signals permafrost thaw, but also creates feedbacks on subsequent thaw by altering the surface energy balance, which may accelerate carbon release from permafrost-affected soils. There are many prior observations of pool growth, but they have typically been locally or regionally focused, and circumpolar analyses are rare. We analyzed recent (2008–2020) time series of sub-meter resolution satellite imagery at 27 survey areas throughout the Arctic to create one of the largest observational records yet of ice wedge thermokarst pool extent. We then analyzed which environmental and meteorological factors have been most strongly associated with recent trends in pool area at the circumpolar scale. Overall, we found evidence for recent pool growth at 44% ( $\pm 15\%$ ) of the survey areas. There was no difference in the recent rate of air temperature increase between sites with and without expanding pools. However, sites with ice wedge thermokarst pool expansion were hillier and had more silt-rich soils than sites with stable or shrinking pools.

© 2024. The Author(s).

This is an open access article under the terms of the [Creative Commons Attribution-NonCommercial-NoDerivs License](https://creativecommons.org/licenses/by/4.0/), which permits use and distribution in any medium, provided the original work is properly cited, the use is non-commercial and no modifications or adaptations are made.

## 1. Introduction

Ice wedge thermokarst pool formation is a key indicator of permafrost degradation. These meter-scale water features (hereafter referred to as thermokarst pools, or simply as pools) develop in pits in the land surface caused by the melting of ice wedges (i.e., buried, meter-scale ice bodies which occupy up to 30% of the upper permafrost volume in non-glaciated tundra) (Kanevskiy et al., 2013). Ice wedges usually occur in net-like spatial patterns,

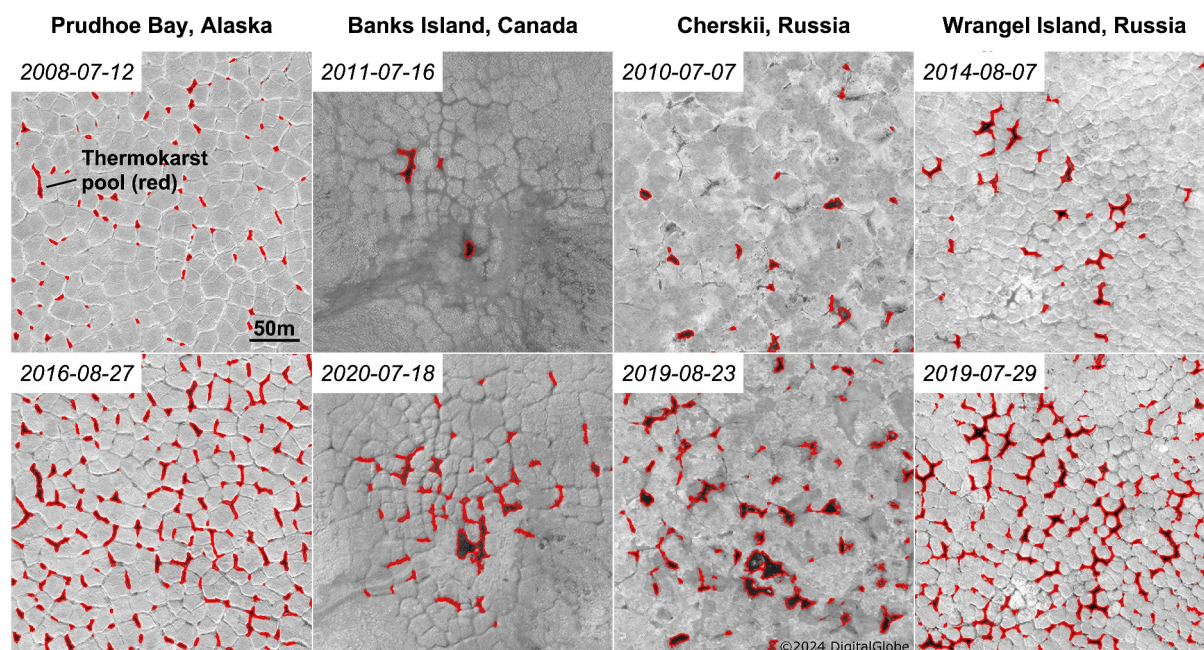


**Figure 1.** Examples of ice wedge thermokarst pool expansion over time spans of 5–9 years in Alaska, Canada, and Russia. Pools are outlined in red within high resolution panchromatic satellite imagery from four survey areas.

developing over centuries through repeated ice vein deposition within a system of near-surface cracks in the ground that open to relieve thermal contraction stresses during severe winters (Lachenbruch, 1962; Leffingwell, 1919). These cracks tend to divide the subsurface into discrete units, which are similar in shape to the desiccation polygons of a dried lakebed but measure 5–30 m across. In many landscapes, this segmentation of the ground is expressed in the highly conspicuous microtopography of high- and low-centered ice-wedge polygons (Abolt & Young, 2020; Mackay, 2000). In other settings, such as hillslopes, the presence of ice wedges may be indiscernible from aboveground, as microtopography tends to be smoothed out by soil creep and other processes (Burn et al., 2021; Liljedahl et al., 2016; Mackay, 1990, 1995). In either type of landscape, permafrost degradation often drives rapid and highly recognizable changes to the ground surface, as localized subsidence above melting ice wedges causes troughs to form within years at the polygon boundaries (Jorgenson et al., 2006; Reynolds et al., 2014). These troughs often fill with water as they deepen, creating a network of variably connected pools (Figure 1).

Besides signaling permafrost degradation, thermokarst pool formation may have a profound impact on subsequent rates of thaw (Abolt et al., 2020; Jorgenson et al., 2006, 2015; Nitzbon et al., 2019; Reynolds et al., 2014). For several decades following their inception, for example, thermokarst pools tend to enhance heat transfer from the atmosphere to the upper permafrost, thereby accelerating thaw (Jorgenson et al., 2006; Nitzbon et al., 2019; Reynolds et al., 2014). Later, as pools become established, the accumulation of an insulating layer of organic matter and other sediment at the bottom of troughs and the growth of reflective, floating mosses at the top of the water column tend to diminish or even reverse this effect (Jorgenson et al., 2015, 2022; Kanevskiy et al., 2017). In recent years, efforts have been made to determine how strongly these feedbacks will impact regional to global-scale rates of permafrost thaw by building the process of thermokarst pool formation into physics-rich land surface models (Aas et al., 2019; Nitzbon et al., 2019, 2020; Painter et al., 2023; Smith et al., 2022). Results to date suggest that pool expansion may accelerate century-scale permafrost thaw in some landscapes to a degree that meaningfully impacts regional carbon budgets, although considerable uncertainty remains. In northeastern Siberia, for example, recent modeling indicates that when both positive and negative feedbacks are accounted for, the presence of thermokarst pools may lead to 4 to 12-fold increase in the mass of permafrost-affected carbon vulnerable to thaw by 2100 (Nitzbon et al., 2020).

To reduce uncertainty in such projections, it is crucial to understand how regimes of thermokarst pool expansion vary throughout the Arctic. To date, this topic is incompletely understood. Although many observations of recent

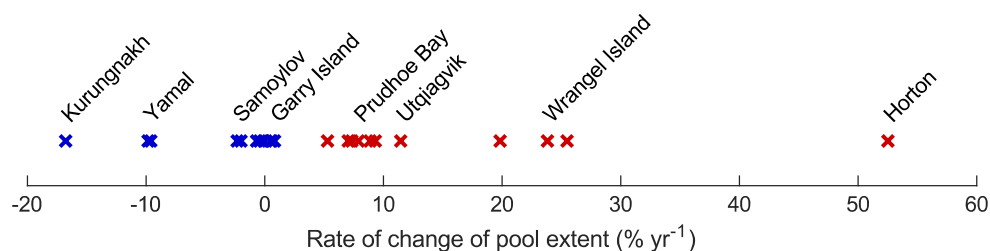


**Figure 2.** Estimated decadal-scale rates of thermokarst pool growth from individual survey areas, calculated using the procedure described in Section 2.3. Red markers denote a positive trend in thermokarst pool extent, while blue markers denote no positive net change. A random subset of survey areas have been labeled by name.

thermokarst pool expansion have been documented, most have been limited in spatial and temporal frequency, relying either on logistically difficult field studies to assess short-term changes (Farquharson et al., 2019; Jorgenson et al., 2006, 2022) or the availability of historic aerial photography to assess multi-decadal changes (Frost et al., 2018; Liljedahl et al., 2016; Reynolds et al., 2014). Compounding this difficulty, conceptual models emerging from recent work have grown increasingly complex. For example, soil core analyses from long-term field sites have revealed a high degree of variability in the strength of negative feedbacks on thermokarst, as some re-stabilized thermokarst troughs have been highly resilient to recent warming, but melting has re-initiated beneath others (Jorgenson et al., 2015, 2022; Kanevskiy et al., 2017). At local to regional scales, there is evidence that vulnerability to thermokarst is highly influenced by factors including geological setting, industrial activity, and fire history (Chen et al., 2021; Reynolds et al., 2014). Outside of disturbed areas, geomorphological position also appears to play an important role. At Banks Island in Canada, for example, Fraser et al. (2018) combined multi-modality remote sensing with field observations to determine that most contemporary thermokarst pool expansion has occurred in upland settings. Based on long-term ground-based measurements, Burn et al. (2021) also found that recent ice wedge degradation has occurred especially rapidly on hillslopes in the western Canadian Arctic. Despite these findings, no investigation at the circumpolar scale has yet revealed systematic relationships between environmental setting and regimes of thermokarst pool dynamics. Without such an analysis, it is impossible to determine which of the relationships identified through earlier fieldwork are most robust across spatial scales, hindering efforts to account for the impact of thermokarst pools on circumpolar permafrost thaw and global climate.

Here we employed a machine-learning-based workflow to quantify the recent net change to thermokarst pool coverage at 27 sites (10–35 km<sup>2</sup> each, covering 400 km<sup>2</sup> total) chosen to represent circumpolar polygonal terrain (Table S1 in Supporting Information S1). Our workflow used a convolutional neural network paired with subsequent image processing operations, taking advantage of submeter-resolution imagery from the WorldView satellites available from approximately 2008–2020. We designed our analysis to determine which factors at the circumpolar scale—including recent air temperature anomalies, soil texture, geomorphological setting, and vegetation dynamics—have been most predictive of spatial variability in recent rates of change to thermokarst pool area. Our analysis revealed instances of thermokarst pool expansion dispersed throughout Arctic North America and Siberia, including in very cold (mean annual air temperature <−13°C) settings (Figure 2, Extended Data Figure 1). Overall, we found that recent departures from long term average air temperatures were no greater at sites with expanding thermokarst pools than at sites with stable or decreasing inundation. Most instances of rapid thermokarst occurred in relatively hilly terrain or in landscapes with silty soils. In flat, lowland terrain, and especially in coastal settings, thermokarst pool extent tended to be stable or even shrinking. These results suggest that, as the Arctic continues to warm, environmental factors including topography and soil texture may be more predictive of spatial variability in pool expansion than rates of air temperature increase.

## 2. Methods

### 2.1. Site Selection and Satellite Imagery Acquisition

The primary data set analyzed in this study was panchromatic imagery from the WorldView satellites, chosen for its high spatial resolution (50 cm or better) and relative temporal abundance. This imagery was acquired from 27 survey areas (Table S1 in Supporting Information S1), which were dispersed throughout all major zones identified

in a previous pan-Arctic map of polygonal tundra (Minke et al., 2007). These zones included North America's Arctic coast between Icy Cape and the Horton River, the northeast Siberian lowlands between the Kolyma and Lena Rivers, and a band stretching across the southern fringes of Siberia's Taymyr Peninsula toward the Gulf of Ob. Additional survey areas outside these regions were included where prominent examples of ice wedge-affected terrain were identified within the online imagery library of the Digital Globe Enhanced View Web Hosting Service (EV-WHS) (<https://evwhs.digitalglobe.com>). A survey area was included only if polygonal troughs were easily discernible in the satellite imagery and the troughs were at least partially inundated due to the presence of thermokarst pools. Although our survey areas were determined primarily based on imagery availability, they included a broad array of topographic settings, climate zones, and soil types, summarized in Table S2 in Supporting Information S1. Some sites, such as Utqiagvik, Samoylov, Anaktuvuk, and Garry Island, were chosen due to long histories of fieldwork, whereas others, such as Taymyr, Yamal, and Wrangel Island, were placed in landscapes where ice wedges have rarely been studied. Survey areas ranged in size from 10 to 35 km<sup>2</sup>, depending on the availability of data. A survey area was considered viable only if a minimum of four panchromatic images with cloud coverage less than 65% were available between 2008 and 2020 from the WorldView1, WorldView2, or WorldView3 satellites, accessed via EV-WHS. In general, imagery from July or August was preferred, as previous work (Chen et al., 2021; Frost et al., 2018; Jorgenson et al., 2015) has demonstrated that thermokarst pool size tends to be most stable during those months—a pattern which we also observed in our own data (Text S1 in Supporting Information S1). However, images from mid to late June or early September were analyzed when other months were unavailable. All images were downloaded in an orthorectified state through EV-WHS and re-projected to 50 cm horizontal resolution in the local UTM coordinate system for subsequent processing.

## 2.2. Thermokarst Pool Mapping

Thermokarst pools were mapped in each image using a machine-learning-based approach, loosely adapted from McAfee et al. (2013). The core of the workflow consisted of two stages. In the first, pixels likely to represent thermokarst pools were identified using a suite of locally trained, five-layer U-Nets for semantic segmentation. The U-Nets were designed to segment imagery into two classes (thermokarst pools and other terrain), and were trained on a subset of WorldView satellite images in which thermokarst pools were manually labeled. For the purposes of this analysis, a thermokarst pool was defined as a body of open water which has developed primarily in the trough at a polygonal boundary, or above an ice wedge. This somewhat restrictive definition excluded other water bodies sometimes associated with thermokarst, such as coalescent center ponds in low-centered polygons, and was chosen to increase confidence that observed decadal-scale increases in thermokarst pool area were associated with ice wedge melting.

Training of the U-Nets was a multi-stage process. In the first stage, a generalized, five-layer U-Net was trained using manually labeled imagery from three of the 27 survey areas (Prudhoe Bay, Kuparuk, and Horton). Subsequently, this generalized U-Net was fine-tuned at each additional survey area using transfer learning, which entailed retraining the weights and biases of the final layers using data which had been manually labeled from the survey area of interest. This workflow was used to quickly generate a highly skilled, site-specific neural network whenever a new survey area was added to the analysis, requiring manageable volumes of new training data which could be quickly generated. Training data was generated by using a thresholding operation on the unprocessed imagery to identify dark objects, then deleting those which did not represent thermokarst pools; the training data from each site comprised <10% of the total imagery to which the mapping procedure was applied.

In the second stage of the workflow, preliminary maps of thermokarst pools generated from the U-Nets were refined using a Fully Connected Conditional Random Field (FCCRF) (Krahenbul & Koltun, 2011). The FCCRF was incorporated to improve segmentation accuracy at the boundaries of thermokarst pools, where the U-Nets tended to underperform. In brief, this refinement was treated as an optimization process, in which the objective function of a solution increased with the number of pixels whose label was reclassified from the U-Net results, but decreased as the variance of pixel intensities within each label (thermokarst pools and other terrain) reduced. This procedure resulted in minor but important changes to the boundaries of the thermokarst pools estimated by the U-Net, improving the alignment between thermokarst pool boundaries and abrupt changes in image intensity (i.e., assuring that boundaries separated dark pixels representing water on one side from lighter pixels representing dry land on the other).

Although the U-Net-FCCRF workflow was generally very skilled, we found that some objects, such as shadows or narrow streams, were frequently mis-identified as thermokarst pools. To correct these errors, results from the workflow were manually reviewed in subsets of one square kilometer and false positives were deleted. We considered this manual editing to be more time efficient than refining the workflow with the goal of full automation. Subsequent to the manual corrections, a validation analysis at two survey areas, employing high-resolution aerial imagery collected near simultaneously to the satellite imagery, revealed that the final maps of thermokarst pools were highly accurate, with 95% of pools by area accurately delineated (Text S2 in Supporting Information S1).

At roughly half the survey areas, the skill of the U-Net was initially impeded due to differences in landscape illumination among images from different dates. To improve the U-Net performance at these sites, a histogram-matching procedure was applied. At each applicable survey area, one date with sharp contrast between pools and bare ground was selected, and the histograms of each remaining image were stretched to recreate a similar level of contrast. At two sites with partly cloudy conditions on one date each, a separate U-Net was employed to mask out clouds, allowing for measurement of thermokarst pool area in cloud-free portions of the imagery (Text S3 in Supporting Information S1).

### 2.3. Analysis of Multi-Year Changes to Thermokarst Pool Extent

Next, we generated a time series of net change to thermokarst pool extent at each survey area. For this study, net change was calculated as change to the cumulative area of all thermokarst pools at a site. We acknowledge that, based on this definition, thermokarst processes may occur even in a site characterized by no net change, as some thermokarst pools may shrink over time due to drainage or infilling with vegetation as other pools simultaneously expand due to permafrost thaw (Frost et al., 2018; Jorgenson et al., 2015; Kanevskiy et al., 2017; Liljedahl et al., 2016). Allowing for this possibility, we identified the prevailing trend in pool extent at each site by estimating the decadal-scale rate of net change, then separating sites experiencing pronounced growth from those with minimal or negative changes to thermokarst pool extent. A set of probabilistic experiments was then conducted to quantify uncertainty in this classification caused by the unequal temporal availability of imagery among survey areas.

We first classified the 22 survey areas in which three or more observations from July to August were available. At each survey area, we calculated a decadal-scale trend in the July and August observations using Theil-Sen linear regression, which was chosen for its robustness against outliers. The average rate of change in thermokarst pool growth was quantified by calculating the slope of the resulting line in units of area per year, then normalizing by estimated pool area in July 2014, the mid-point in the time domain. This calculation resulted in an estimated growth rate in units of percent change per year. As the analysis revealed a gap centered at about 3% growth per year, this threshold was used to separate sites with evidence of pronounced thermokarst pool growth from sites with stable or shrinking thermokarst pool extent (Figure 2).

It is important to note that, although we observed significant spread in estimated growth rates among sites where pool growth was identified, we interpreted this variability as having limited physical meaning. This is because, when pool growth did occur, it tended to follow a non-linear trajectory, which caused estimated rates of change to be highly sensitive to the start and end dates over which they were calculated. For example, although Prudhoe Bay provided one of the most extreme examples of thermokarst seen in our data set, it ranked only eighth out of 11 sites with positive rates of pool expansion, as nearly all the growth was concentrated in a single year. Acknowledging this limitation, we employed the regression analysis described above only as a tool for binary classification.

Finally, at the five survey areas with fewer than three midsummer (i.e., July or August) observations, classification was based on manual interpretation of the results. At four of these sites (Ikpikpuk, Khatanga, Taymyr, and Yana), there was no discernible trend in thermokarst pool extent, either positive or negative, regardless of the months in which observations were made. However, we considered the evidence for thermokarst pool expansion compelling at one survey area (Brooks Foothills), where pool extent increased monotonically over three observations between 2013 and 2020, each made within a narrow early summer window between June 13 and June 19. Moreover, the growth of individual thermokarst pools at this site correlated positively with topographic convexity. As described in Section 4.1, this finding is compatible with conceptual models of ice wedge melting on hillslopes, but not compatible with the explanation that pool growth was due merely to wetter conditions.

#### 2.4. The Effect of Temporal Sample Size on Survey Area Classification Accuracy

Following the classification of each survey area as experiencing pronounced thermokarst pool growth or no net change, we explored the effect of the number of available satellite observations on classification outcomes through a probabilistic experiment. We began by identifying the five sites with the greatest number of observations made in the months of July and August. These included Herschel Island, Wrangel Island, Isachsen, Prudhoe Bay, and Nechilik, each of which had six or more midsummer data points. Operating on the assumption that these five sites were correctly identified as experiencing or not experiencing pronounced thermokarst pool growth, we then repeated our classification procedure at each of them, substituting every possible subsample of three, four, or five observations. We found that, depending on subsample size, the resulting re-classification agreed with the original decision 77%–90% of the time (Figure S1a in Supporting Information S1). To quantify uncertainty in our estimate of the total number of survey areas which experienced thermokarst pool expansion, we then conducted 1 million probabilistic simulations, in which every survey area with only three, four, or five observations was randomly reclassified, based on these rates of accuracy. The results suggested that, on average, three survey areas may presently be mis-classified due to insufficient data. 85% of the time, four sites or fewer were estimated to be mis-classified (Figure S1b in Supporting Information S1).

#### 2.5. Analysis of Environmental Factors Impacting Landscape-Scale Thermokarst Pool Dynamics

After distinguishing between survey areas with and without evidence for net thermokarst pool expansion, we employed a set of one-tailed Wilcoxon rank sum tests to quantify how strongly several environmental factors were associated with this classification. These factors included recent air temperature trends, mean annual ground temperature at the top of permafrost, topographic setting, soil properties, and trends in vegetation growth as quantified by the normalized difference vegetation index (NDVI).

Historic air temperature data at each site were downloaded from the MERRA-2 climate reanalysis product (NASA GMAO, 2015) at hourly resolution from 1 January 1980 to 31 October 2020. At each survey area, mean annual air temperature was calculated as the mean air temperature from 1 January 1980 to 31 December 2009, comprising a 30-year record. Additionally, thaw-degree-days (TDD) and freezing-degree-days (FDD) were calculated each summer and winter as the time-integral of air temperatures above and below freezing, respectively. Mean annual ground temperature at each site, expressed as an average value at the top of the permafrost between 2000 and 2016, was extracted from a circumpolar map generated by Obu et al. (2019).

Topographic data for each survey area were downloaded at 10 m horizontal resolution from ArcticDEM (Porter et al., 2018), which is derived from photogrammetric analysis of imagery from the WorldView satellites. We selected this data set as it covered all 27 survey areas. Topographic attributes calculated at each survey area included mean elevation above sea level and the amount of topographic relief present, expressed as the range in observed elevation. To account for the effect of survey area size, the calculations of topographic relief were normalized using a simple procedure. One hundred overlapping boxes that were two by four kilometers (the largest shape which fit within the boundaries of each survey area) were randomly drawn throughout the landscape, and normalized topographic relief was calculated as the mean range in elevation observed within the boxes.

Soil texture data were extracted from the SoilGrids 2.0 database (Poggio et al., 2021), which maps soil properties globally at 250 m resolution. At each survey area, we extracted the mean silt content and mean clay content as a mass percentage of total mineral content at two depth intervals: Surface to 1 m (roughly corresponding to the active layer) and 1–2 m (roughly corresponding to the top of the permafrost). Our choice of these variables was motivated by observations that thermokarst processes tend to be strongest in areas with high ice content (Farquharson et al., 2016; Frost et al., 2018) and the inference from thermal contraction theory that fine sediments are most favorable for ice wedge growth (Lachenbruch, 1962). Finally, the “greening” or “browning” of each survey area was quantified as the rate of change of maximum annual NDVI, extracted from pre-computed global rasters derived from the MODIS satellite (Didan, 2021). We examined these data based on the crucial role that vegetation growth plays in stabilizing feedbacks on pool growth, which we hypothesized might be visible from space.

## 2.6. Analysis of Growth Rates in Individual Thermokarst Pools

Within individual survey areas, fine spatial scale variability in thermokarst pool growth was assessed by tracking how the areas of individual pools changed over time. At each survey area, pool area on one date from the first half of the study period was compared with a later observation from the second half. Quantifying pool-level expansion or shrinkage required matching pools in the imagery from the earlier date with pools observed at the later date, which was accomplished through one of three procedures. At six survey areas (Prudhoe, Brooks Foothills, Jago, Anaktuvuk, Tapkaurak, and Kuparuk), the orthorectification of the satellite imagery was precise enough to allow for accurate co-registration of early and late images using simple translation of the later image. At five additional sites (Anadyr, Banks Island Site 1, Icy Cape, Nechilik, and Yana), simple translation was inadequate for thermokarst pool matching, but accurate results were obtained using registration with an automated approach known as “diffeomorphic demons” (Vercauteren et al., 2009), which allows for non-uniform displacement between the earlier and later images. At the remaining survey areas, pools in the early image were matched manually with pools in the later image. For a given site, the growth of each pool present in the earliest image was assessed by calculating the area of all overlapping pools in the later image. Where multiple pools in the earlier image coalesced into a single pool, the area of the later pool was divided and assigned to the earlier pools in proportion to their original areas.

Motivated by recent findings that polygonal troughs in uplands and on hillslopes have been especially vulnerable to thermokarst in recent years (Burn et al., 2021; Fraser et al., 2018), we then assessed whether rates of change to thermokarst pool area varied systematically with geomorphological position, quantified by topographic convexity. Convexity was calculated as the negative Laplacian of elevation, after smoothing a survey area's DEM using a filter with a radius of 50 m, to reduce the effects of polygonal microtopography. At each site, individual thermokarst pools were grouped into 10 bins according to topographic convexity at their centroid. A one-tailed Kendall rank correlation test was used to determine whether the area weighted mean rate of change to pool area within a bin correlated with convexity. Both a left- and a right-tailed test were performed at each study area, to test for both positive and negative relationships.

## 3. Results

### 3.1. Environmental Factors Associated With Inter-Site Variability in Thermokarst Pool Dynamics

Our analysis revealed instances of thermokarst pool expansion throughout the circumpolar region (Figure 3). Accounting for observational biases through the probabilistic uncertainty analysis described in Section 2.4, we estimate with 85% confidence that pronounced thermokarst pool expansion occurred at  $12 \pm 4$  of the 27 landscapes examined. At the survey areas most likely to have experienced expansion, the percent growth in pool extent between the earliest and latest observations varied from 40% to 500%. The time series of thermokarst pool extent at each of the 27 survey areas are shown in Figure 4.

By far, the most significant environmental factors which distinguished sites with evidence for thermokarst pool expansion were those related to topography. Normalized topographic relief, quantified as the mean range in elevation observed within 100 eight-square-kilometer regions dispersed randomly throughout a survey area, was strongly associated with pool expansion, as the survey areas classified as experiencing net increases were typically found in hillier settings (median normalized topographic relief = 54 m, interquartile range (IQR) = 34–74 m) relative to survey areas without evidence of net change (median = 21 m, IQR = 17–26 m) ( $p$ -value < 0.01, one-tailed Wilcoxon rank sum test) (Figure 5a). At the pan-Arctic scale, survey areas classified as experiencing pronounced increases to thermokarst pool area were also found at higher mean elevations above sea level (median = 97 m, IQR = 39–135 m) than survey areas without evidence of net change (median = 15 m, IQR = 8–23 m) ( $p$  < 0.01). This second finding reflects that lower elevation survey areas also tended to be the flattest, occurring in settings such as coastal plains or river deltas.

To a lesser degree, we found that sites with expanding thermokarst pools were distinguished by increased silt content beneath the active layer. Sites experiencing pool expansion had modestly higher silt content below a depth of 1 m (median = 41% by mass, IQR = 35%–43%), or roughly at the top of the permafrost, relative to sites without evidence of pool growth (median = 34%, IQR = 26%–42%) ( $p$  < 0.05) (Figure 5b). No significant difference was identified in silt content at less than one m of depth or clay content at either depth interval. Likewise, no significant difference was detected in the total content of fines (silt + clay) at either interval.

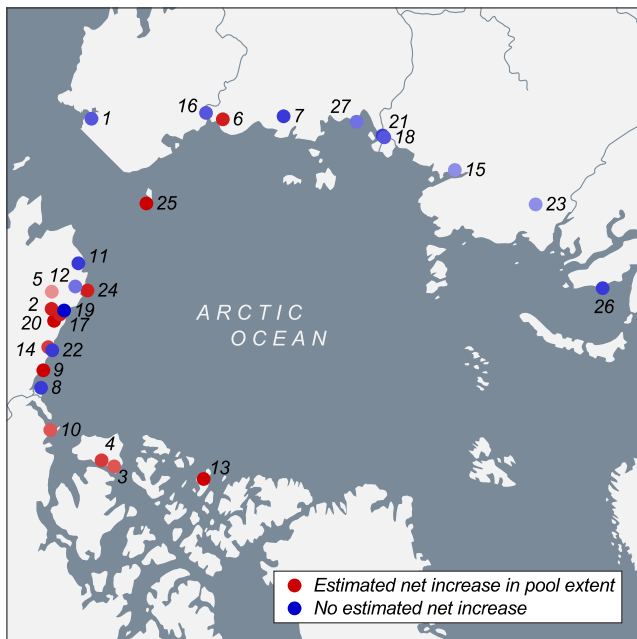


**Figure 3.** Survey areas in the present analysis, colored according to whether or not a clear net increase in thermokarst pool extent was observed. Numbers correspond with site labels in Table S1 in Supporting Information S1. Color intensities deepen with the number of July and August observations, also reported in Table S1 in Supporting Information S1.

We found no significant difference in mean annual air temperature between sites with expanding thermokarst pools (median =  $-9.8^{\circ}\text{C}$ , IQR =  $-12.6$  to  $-9.1^{\circ}\text{C}$ ) and those with no evidence of change (median =  $-9.8^{\circ}\text{C}$ , IQR =  $-12.6$  to  $-8.0^{\circ}\text{C}$ ) (Figure 5c). Likewise, no significant difference was detected in mean annual temperature at the top of the permafrost (median =  $-7.5^{\circ}\text{C}$  and  $-7.1^{\circ}\text{C}$ , IQR =  $-10.4$  to  $-6.8^{\circ}\text{C}$  and  $-9.5$  to  $-5.8^{\circ}\text{C}$  respectively). Notably, each of the three coldest survey areas in our analysis, all in the Canadian High Arctic and with mean annual air temperatures below  $-13^{\circ}\text{C}$ , experienced pronounced increases in thermokarst pool area in the past decade. This finding adds to a growing body of observations of abrupt ice-wedge degradation in very cold settings (Farquharson et al., 2019; Fraser et al., 2018; Jorgenson et al., 2006), where it had earlier been presumed that permafrost would be relatively resilient to climate change.

We also found that recent air temperatures (i.e., during the time period from which satellite observations were available at each site) were no higher above long-term averages at survey areas with evidence of expanding thermokarst pools than at those without evidence for positive net change. This finding held true whether quantified in terms of percent change to thaw-degree-days (the time integral of temperatures above freezing during summer, which increased by 7.8% and 8.7% at survey areas with and without net change, respectively) (Figure 5d) or freezing-degree-days (the converse integral in winter, which decreased by 7.2% and 5.5%) (Figure 5e).

To the extent that they were observable from space, trends in vegetation growth, quantified by the rate of change of maximum annual NDVI at each site during the time period of satellite observations, were not associated with thermokarst pool expansion. We found no significant difference in rates of greening among sites with expanding pools (median =  $4 \times 10^{-3} \text{ yr}^{-1}$ , IQR =  $-2 \times 10^{-3}$  to  $5 \times 10^{-3} \text{ yr}^{-1}$ ) and sites without evidence of pool growth (median =  $2 \times 10^{-3} \text{ yr}^{-1}$ , IQR =  $3 \times 10^{-3}$  to  $5 \times 10^{-3} \text{ yr}^{-1}$ ) (Figure 5f).

### 3.2. Local-Scale Variability on Thermokarst Pool Growth Within Individual Survey Areas

Our analysis of intra-site variability in thermokarst pool expansion revealed that rates of change to pool area were significantly correlated ( $p < 0.05$ , one-tailed Kendall rank correlation test) with topographic convexity at 10 of the 27 survey areas (Figure 6). At all 10 sites with statistically significant results, the direction of the correlation was positive, meaning that the fastest growing pools were in convex locations such as hilltops. Notably, this correlation was not limited to sites that experienced an overall net increase in pool area. At Anadyr and Nechilik, for example, thermokarst pool expansion at topographically convex points in the landscape was balanced by shrinkage in concave regions, resulting in no net change to landscape-scale thermokarst pool extent.

## 4. Discussion

### 4.1. Pedologic and Topographic Factors Associated With Thermokarst Pool Expansion

Overall, the comparison between our study areas highlighted that a combination of environmental factors has controlled circumpolar variability in recent thermokarst pool expansion. Although thermokarst is triggered by thermal disturbance to ice-rich permafrost, we found that, from 2008 to present, spatial variability in the rate of change of air temperatures across the Arctic mattered far less than variability in the local terrain, particularly with regards to topography and soil texture.

Our finding of increased silt content at depth within landscapes experiencing pool expansion may reflect several factors. One is the increased potential for thermokarst in settings with large and abundant ice wedges, since wedge ice develops most readily in fine sediments such as silt, as opposed to coarser material such as sand and gravel (Farquharson et al., 2016; Frost et al., 2018; Lachenbruch, 1962). Although ice wedge melting does not always cause thermokarst pools to form, the presence of large ice wedges maximizes the potential for pool growth when



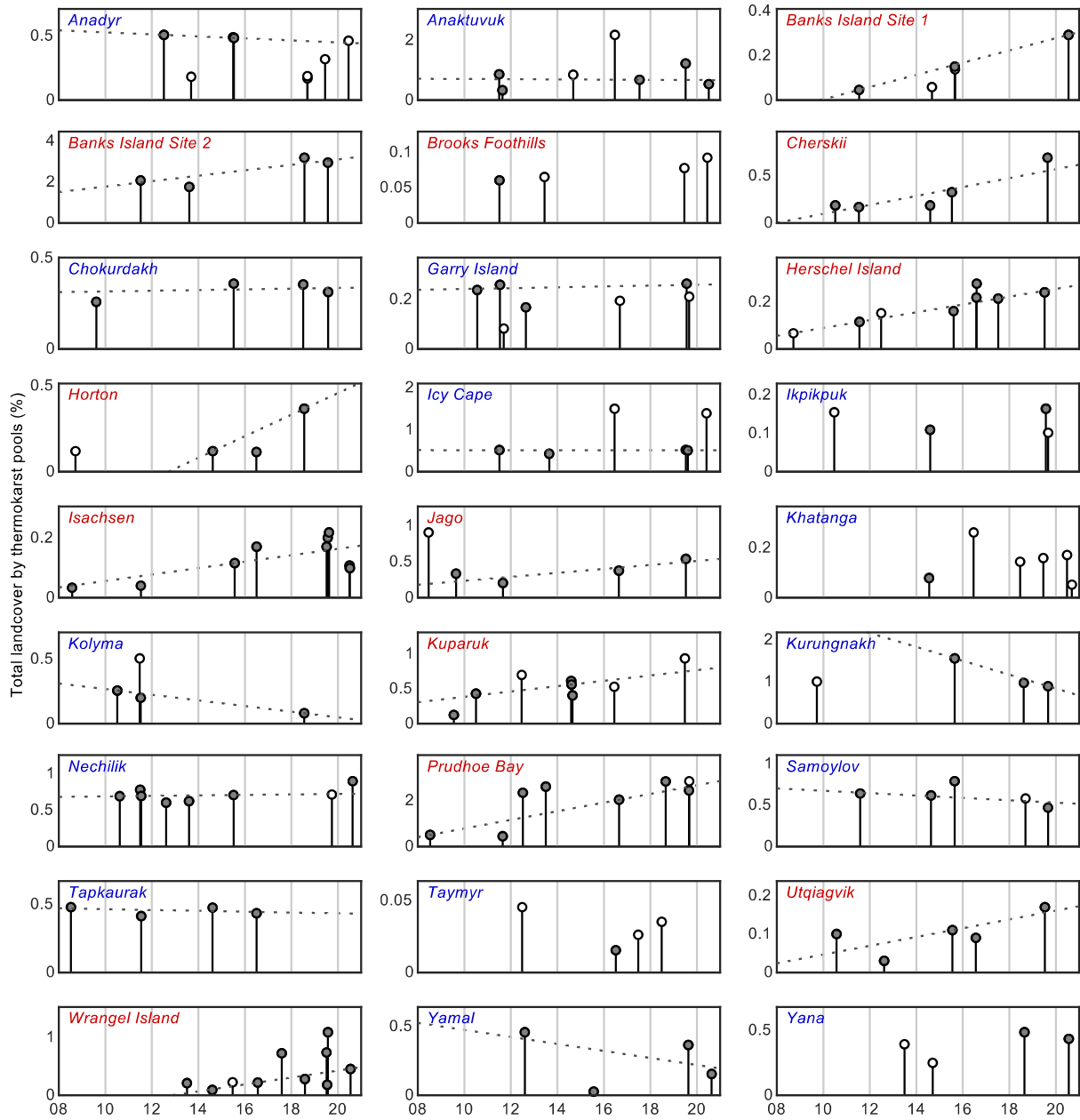


**Figure 4.** Time series of thermokarst pool extent at each survey area. Red text indicates sites classified as experiencing a net increase to thermokarst pool extent during the time period from which satellite data were available; blue text indicates that no trend was identified, using the procedure described in Section 2.3. Dark markers indicate that an observation was made during the months of July or August, while white markers indicate the observation was made in mid-to-late June or early September. Dashed lines indicate decadal-scale growth trajectories calculated using Theil-Sen regression at sites with more than three observations from July or August.

permitted by local hydrologic conditions. Aside from the size of the ice wedges themselves, the high concentration of ice lenses and other forms of segregated ice in silty soils may also increase the potential for thermokarst pool formation, as the melting of these smaller ice bodies would contribute to subsidence in the soils above and directly adjacent to an ice wedge. It is plausible, for example, that a thermokarst pool may initially form in a depression caused by the melting of ice lenses, before positive feedbacks cause thaw to penetrate an underlying ice wedge. By contrast, we observed that thermokarst pools in coarse deposits—such as those at the Ikpikpuk survey area, which overlies a Pleistocene sand dune complex—occupied only a small fraction of the land surface and did not grow appreciably in recent years.

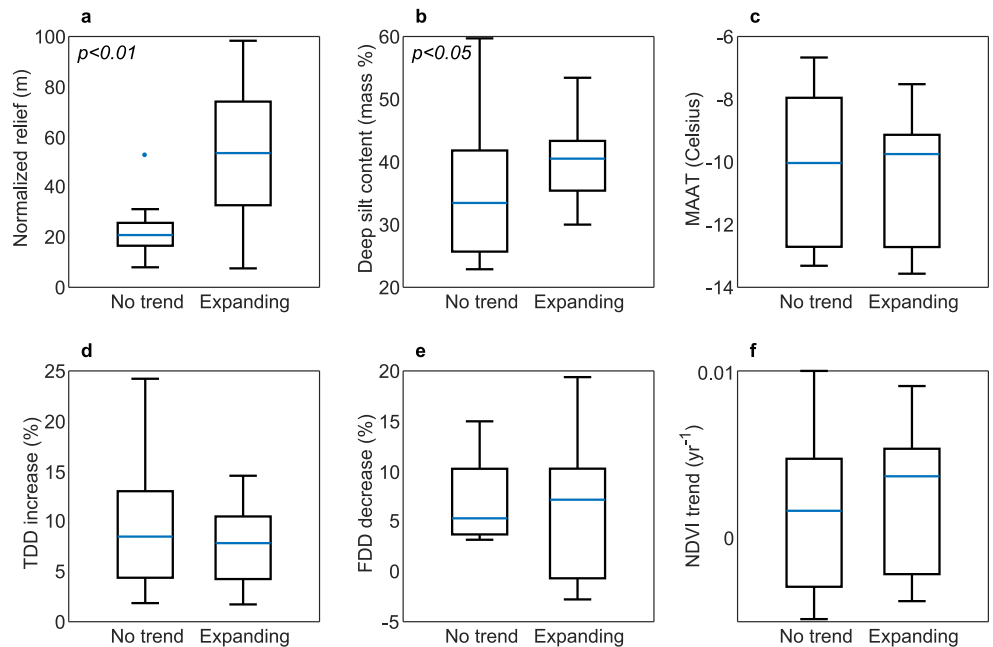


**Figure 5.** Boxplots comparing sites with and without a net increase in thermokarst pool extent, in terms of (a) normalized topographic relief, (b) silt content by mass below a soil depth of 1 m, (c) mean annual air temperature, (d) the extent to which summer thaw-degree-days (TDD) were above average during the interval from which satellite imagery was available, relative to 1981–2010, (e), the extent to which winter freezing-degree-days (FDD) were below average over the same interval, and (f) rates of greening during the study period, quantified as trends in maximum annual normalized difference vegetation index. Inset  $p$ -values correspond to results from a one-tailed Wilcoxon rank sum test to distinguish difference between site classes. Note. For visualization purposes, the plot for expanding sites in panel (d) does not include Wrangell Island, where the recent increase to TDD is an outlier at more than 100%.

The positive relationship we observed between macroscale topographic relief and thermokarst pool expansion suggests an increased vulnerability to climate change of polygonal ground in hilly landscapes. This also is potentially the result of many factors, but one explanatory mechanism is that hillslopes, unlike lowlands, are prone to diffusive soil erosion, which reduces the thermal buffer between the tops of the wedges and the atmosphere, even if it occurs at slow rates (i.e., centimeters or fewer per century) and leaves no perceptible scars at the ground surface (Gilbert, 1909; McKean et al., 1993). Even prior to the onset of thermokarst, the tops of the anti-syngenetic ice wedges which develop in these settings tend to be sharply truncated by the active layer (Mackay, 1990, 1995), whereas ice wedges beneath stable or aggrading land surfaces are commonly overlain by several decimeters of perennially frozen sediments known as the intermediate layer (Shur et al., 2005). Recent observations at Banks Island in the Canadian Arctic have linked the lack of an intermediate layer in anti-syngenetic wedges with increased vulnerability to climate change (Fraser et al., 2018). Although we lack direct field observations to verify the presence of anti-syngenetic ice wedges, our data are compatible with this conclusion, as trends we observed in the growth of individual pools revealed a significant correlation ( $p < 0.05$ ) between topographic convexity and pool expansion at 10 of the 27 survey areas, which was positive whenever observed (Figure 6). In other words, we found that the individual pools most prone to expansion were those located in convex locations such as hilltops, which are precisely where net soil removal and anti-syngenetic ice wedges are most likely to occur.

#### 4.2. Pool Drainage in Hilly Landscapes With Well-Connected Troughs

Despite the overall positive correlation between topographic relief and pool expansion, we also observed a competing effect, whereby hilly terrain may inhibit pool growth when troughs become sufficiently connected to allow lateral drainage. This process was exemplified at the Anaktuvuk survey area, located in the foothills of Alaska's Brooks Range, where no decadal-scale net change to thermokarst pool area was observed, despite the well-documented occurrence of ice wedge melting throughout the past decade, spurred by a wildfire in 2007 (Jones et al., 2015; Rettelbach et al., 2021). Instead of demonstrating a multi-year trend, thermokarst pool area at

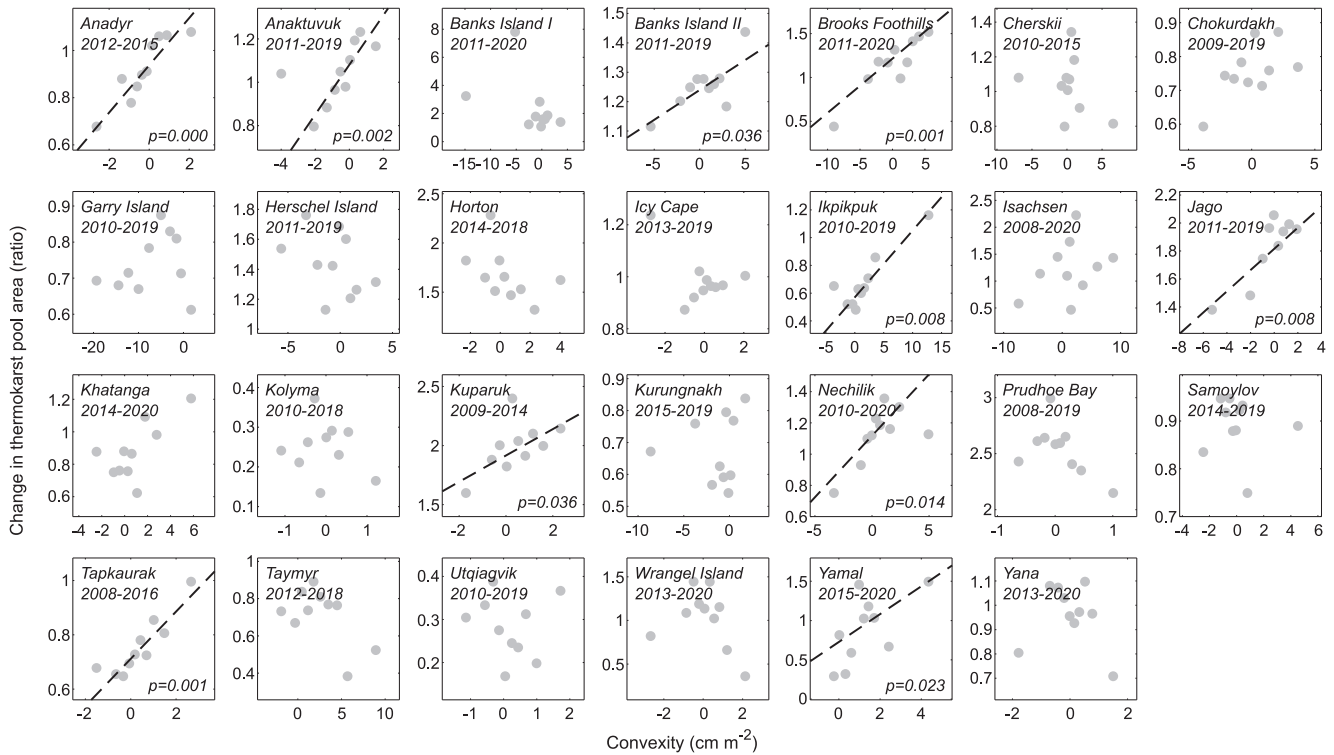


**Figure 6.** Relationship between topographic convexity and individual pool growth at each survey area. Dots represent area-weighted mean pool growth after grouping all pools at a site into 10 equally sized bins by convexity. Lines represent best linear fit using Thiel-Sen regression, and  $p$ -values refer to the results from a one-tailed Kendall rank correlation test, evaluating whether a trend was present. Convexity was calculated at thermokarst pool centroids after smoothing topography using a filter with a radius of 50 m, to reduce the effects of polygonal microtopography.

the survey area was characterized by extreme fluctuations—typically comprising only a small fraction of the land surface, but spiking during one observation from the early summer in 2016, when pools in concave landscape positions coalesced into a conspicuous series of drainage networks (Figure 7).

The fluctuating behavior of thermokarst pool extent at Anaktuvuk differs markedly from conceptual models developed in flatter landscapes. However, it mirrors recent observations of a widespread onset of thermokarst trough formation on hillslopes of the western Canadian Arctic, where the surface remained largely dry, as surface water tended to drain down-slope through the trough network (Burn et al., 2021). Field observations from this region suggest that the relative dryness of the soils may in fact have increased the vulnerability of the underlying ice wedges, by reducing the latent heat consumed during seasonal thaw, resulting in a thicker active layer. Our observations suggest that, at similar hilly sites throughout the Arctic, pools may form abruptly following snowmelt or summer rainstorms, but tend to diminish over timespans of days to weeks due to lateral drainage (Figure 8). Besides at Anaktuvuk, this behavior was observed in the upper Jago River watershed of Alaska, where thermokarst pool area spiked in June 2008, and in the mountainous terrain of Wrangel Island in Siberia, where two flash-inundation events were observed in rapid succession in July 2019. In satellite images acquired during these events, otherwise isolated thermokarst pools were interconnected by a web of dark troughs whose orientation aligns with the topographic gradient, offering strong evidence of surface or near-surface drainage (Figure S2 in Supporting Information S1). Due to the ephemeral nature of thermokarst pools in these settings, feedbacks on thaw, either positive or negative, should not be expected to follow the same trajectories that have been observed in lowland terrain.

### 4.3. Meteorological Trends and Recent Thermokarst History

Despite the poor capacity for air temperature records alone to predict circumpolar patterns in recent pool dynamics, we observed instances in which thermokarst pool expansion aligned clearly with extreme meteorological events. At Prudhoe Bay, for example, where reliable precipitation data were available, a well-defined pulse of

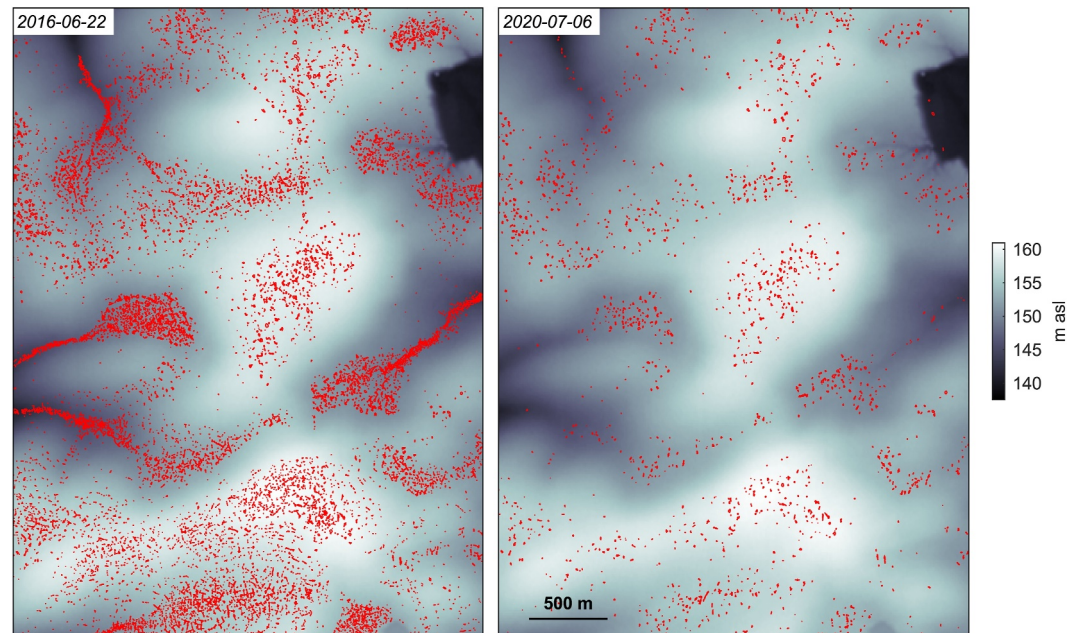


**Figure 7.** Thermokarst pools at the Anaktuvuk survey area during a wet, early summer (left) and dry, mid-summer (right) observation, plotted over a digital elevation model from ArcticDEM.

pool expansion between the summers of 2011 and 2012 coincided with above average air temperatures and an exceptional amount of snowfall during the autumn of 2010; and at Wrangel Island, a fluctuating but increasing trend in pool area toward the end of the decade was preceded by several remarkably warm summers (Text S5 in Supporting Information S1). The example from Prudhoe Bay complements a body of modeling and field-based studies demonstrating that extreme precipitation events may trigger thermokarst, either by delivering heat to the permafrost through advective transport or altering energy exchange between the atmosphere and the ground surface (Jorgenson et al., 2015; Magnusson et al., 2022; Mekonnen et al., 2021; Nitzbon et al., 2019, 2020, 2021). We did not investigate variability in precipitation regimes among our field sites due to a lack of reliable historical records with circumpolar coverage, though we suggest further research into links between precipitation, ice wedge melting, and thermokarst pool expansion is warranted.

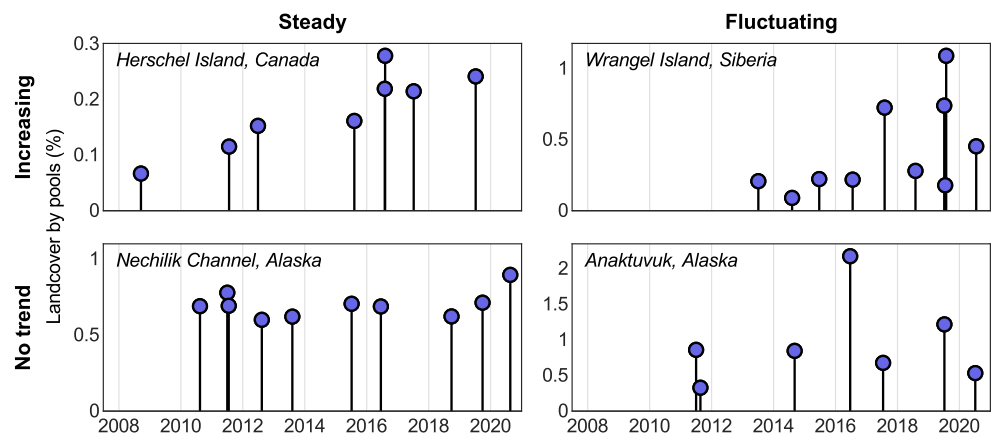


**Figure 8.** Four regimes of recent thermokarst pool dynamics. Flashy (i.e., fluctuating) regimes are often observed at sites where troughs are well-connected and occur on a sloping surface. Thermokarst pool extent in landscapes that either are flat or contain poorly connected trough networks is often steady or steadily increasing.

#### 4.4. The Circumpolar Prevalence of Negative Feedbacks on Thermokarst Pool Growth

Another major control on the relationship between rising air temperatures and thermokarst pool expansion is the local history of ice wedge melting and restabilization, as negative feedbacks on thaw, caused primarily by vegetation growth, must be accounted for in landscapes where pools have persisted at decadal timescales. Additional context regarding this factor is available from several field sites in Arctic Alaska, where prior analyses of historical aerial photography demonstrate that a climate-change-driven expansion of thermokarst pools began as early as the 1940's (Frost et al., 2018; Jorgenson et al., 2006, 2022; Liljedahl et al., 2016). In the past two decades, observations of soil cores from the same landscapes have frequently demonstrated recovery of the intermediate layer atop degraded ice wedges caused by the accumulation of new organic material (Jorgenson et al., 2006, 2015, 2022; Kanevskiy et al., 2017), providing direct evidence of thermokarst stabilization, even as the climate has continued to warm. Our data indicate that this stabilizing trend is common not only in Alaska but in lowland settings throughout the Arctic, where individual thermokarst pools commonly shrank, even as other pools in the same landscapes expanded (Figure 6). In many such cases, rates of change to pool area varied systematically across a landscape, with the greatest likelihood of growth near hilltops. At Ikpikpuk, Nechilik, Yamal, and Anadyr, for example, recent pool expansion in convex landscape positions was balanced by pool shrinkage in concave settings. At other lowland sites including Chokurdakh, Utqiagvik, and Garry Island, we found that most of the individual thermokarst pools which were already present in the summers of 2009 and 2010 shrank throughout the following decade, but total thermokarst pool extent remained stable due to the formation of new pools. These observations point to highly dynamic conditions of permafrost thaw and recovery, even in settings that might be classified as stable if only the total degree of surface inundation is considered. The prevalence of individual pool shrinkage at the circumpolar scale affirms that the robustness with which negative feedbacks stabilize the thermal regime above partially degraded ice wedges will be a major control on future trajectories of thermokarst pool extent.

#### 4.5. Limitations of the Present Study

As mentioned in a prior section, one important limitation to the present study is the lack of reliable precipitation records at the majority of our survey areas. This constraint precluded us from testing the hypothesis that changing rainfall and snowfall regimes may be predictive of circumpolar variability in thermokarst pool expansion, which merits investigation, given the influence that extreme precipitation events have on permafrost degradation. Another problem stemming from the lack of precipitation data is that, based on remote sensing analysis alone, we cannot fully exclude the possibility that some of our observations of high thermokarst pool extent may reflect unusually wet conditions, rather than permafrost thaw. While we acknowledge this limitation, we sought to curtail its impact on our conclusions through our analysis of monthly trends in thermokarst pool extent (Text S1 in Supporting Information S1), which reproduced earlier work demonstrating that pool extent tends to be smallest and most stable in the months of July and August (Chen et al., 2021; Frost et al., 2018; Jorgenson et al., 2015), and supported our decision to rely primarily on observations from these months to detect decadal-scale trends in area. We also note that our observation that rates of change to pool area often varied systematically throughout a survey area, with some thermokarst pools growing even as others in the same landscape shrank, is incompatible with the hypothesis that precipitation was the main driver of variability in pool extent at these sites. To better parse the influence that influence of precipitation on thermokarst pool dynamics, we suggest that future work applying our methodology to landscapes with long term, ground-based precipitation records is warranted.

Another limitation to our study is that, because many of the survey areas were in remote regions, inter-site comparisons depended on circumpolar data products which are less reliable than direct field observations. For example, our finding that expanding thermokarst pools were more common in silty soils was based on a soil texture data product which extrapolates relatively sparse Arctic observations across a 250 m grid. While we interpret this result as demonstrating that pool development is more likely in soils rich with syngenetic ice and containing large ice wedges, only observations of the subsurface can directly confirm this conclusion. Similarly, our conclusion that syngenetic ice wedges are among the most vulnerable to climate change at the circumpolar scale was based on interpretation of topographic evidence, but would be strengthened by analysis of cores taken directly from sites such as Brooks Foothills or Nechilik, where the fastest expanding pools were located near hilltops. Despite these limitations, our central finding, that rates of thermokarst pool expansion vary systematically with topographic and soil texture data which is already available at the circumpolar scale, provides context

that is immediately useful for parameterizing and validating land surface models used to account for the impact of pool growth on the global carbon cycle. It also provides a starting point for future field campaigns, which might collect more complete meteorological, pedological, and botanical data to complement remotely sensed observations of thermokarst pool extent.

A final limitation is that, while our sites included a broad variety of topographic, pedologic, and climatic settings, survey area selection was not truly random, but rather conducted through manual selection of ice-wedge-affected landscapes with adequate image availability. As the total spatial extent of Arctic terrain underlain by ice wedges is currently unknown, we cannot precisely quantify how representative our survey areas are. One method to address this limitation in the future may be further development to improve the accuracy of our pool detection algorithm—either through expansion of the training data set, or alteration of the neural network architecture—to reduce or eliminate the need for manual deletion of false positives. A fully automated workflow would enable the processing of much broader spatial domains, potentially approaching the entire Arctic land surface, which would permit more robust testing of the patterns detected in this investigation.

## 5. Conclusions

Among 27 field sites dispersed through Alaska, Canada, and Russia, we found that recent thermokarst pool expansion was most common in landscapes characterized by hilly terrain and silt-rich soils at depth. This conclusion builds on a large body of prior field studies and remote sensing investigations, demonstrating that certain locally to regionally observed patterns in ice wedge thermokarst pool development are applicable throughout the circumpolar domain. At the pan-Arctic scale, recent trends in air temperature did not explain spatial variability in pool growth. The increased vulnerability to pool expansion of landscapes with silty soils is consistent with the tendency for large and abundant ice wedges to develop in fine-grained sediments. A positive correlation between growth in individual pools and local topographic convexity suggests that ice wedges in hilly landscapes may be more vulnerable to climate change than other ice wedges due to net soil loss from diffusive erosion, which reduces the thermal buffer between the atmosphere and the top of the ice wedges. In settings characterized by high topographic relief and sufficient trough connectivity, lateral drainage in the troughs causes fluctuating or flashy trends in thermokarst pool extent, which diverge from the progression of thermokarst in flatter terrain. In lowland settings spanning the Arctic, pool shrinkage was common over the past 10–15 years, even as new thermokarst pools formed in the same landscapes. This finding suggests many of the pools present at the start of our analysis were already in the process of stabilizing, which may contribute to the lack of a clear pan-Arctic relationship between historic air temperature records and thermokarst pool growth.

## Data Availability Statement

The primary data sets analyzed and generated during this study, including all commercial satellite imagery and derived maps of thermokarst pools, have been uploaded with permission of the private vendor to a repository in the Environmental System Science Data Infrastructure for a Virtual Ecosystem (Abolt et al., 2024). All additional data sets analyzed during this study are available through public repositories (Boike et al., 2015; Didan, 2021; McAfee et al., 2013; NASA GMAO, 2015; Obu et al., 2019; Porter et al., 2018).

Novel code from this analysis, including workflows for mapping thermokarst pools (Abolt et al., 2024) and segmenting clouds from WorldView satellite imagery (Rumpca et al., 2024), has been uploaded to two repositories in the Environmental System Science Data Infrastructure for a Virtual Ecosystem.

## Acknowledgments

Support for this research included the Next Generation Ecosystems Arctic (NGEE-Arctic) project (DOE ERKP757) funded by the Office of Biological and Environmental Research in the U. S. Department of Energy Office of Science. GG and IN were supported by the project HGF AI-CORE. TR was supported by GeoX and HEIBRiDS. CJA was supported by the Laboratory Directed Research and Development program of Los Alamos National Laboratory under project number 20200771PRD4.

## References

- Aas, K. S., Martin, L., Nitzbon, J., Langer, M., Boike, J., Lee, H., & Westermann, S. (2019). Thaw processes in ice-rich permafrost landscapes represented with laterally coupled tiles in a land surface model. *The Cryosphere*, 13(2), 591–609. <https://doi.org/10.5194/tc-13-591-2019>
- Abolt, C. J., Atchley, A. L., Harp, D. R., & Rumpca, C. T. (2024). Maps of ice wedge thermokarst pool expansion at twenty-seven circumpolar survey areas [Dataset]. *Environmental System Science Data Infrastructure for a Virtual Ecosystem*. <https://doi.org/10.5440/1834773>
- Abolt, C. J., & Young, M. H. (2020). High-resolution mapping of spatial heterogeneity in ice wedge polygon geomorphology near prudhoe bay, Alaska. *Scientific Data*, 7(1), 87. <https://doi.org/10.1038/s41597-020-0423-9>
- Abolt, C. J., Young, M. H., Atchley, A. L., Harp, D. R., & Coon, E. T. (2020). Feedbacks between surface deformation and permafrost degradation in ice wedge polygons, arctic coastal plain, Alaska. *Journal of Geophysical Research: Earth Surface*, 125(3), e2019JF005349. <https://doi.org/10.1029/2019jf005349>
- Boike, J., Voh, G., Stoof, G., Sachs, T., Busse, H., & Muster, S. (2015). Near-infrared orthomosaic of samoylov island, siberia, summer 2014 (854 mb) [Dataset]. *PANGAEA*. <https://doi.org/10.1594/PANGAEA.845723>

- Burn, C. R., Lewkowicz, A. G., & Wilson, M. A. (2021). Long-term field measurements of climate-induced thaw subsidence above ice wedges on hillslopes, western arctic Canada. *Permafrost and Periglacial Processes*, 32(2), 261–276. <https://doi.org/10.1002/ppp.2113>
- Chen, Y., Lara, M. J., Jones, B. M., Frost, G. V., & Hu, F. (2021). Thermokarst acceleration in Arctic tundra driven by climate change and fire disturbance. *One Earth*, 4(12), 1718–1729. <https://doi.org/10.1016/j.oneear.2021.11.011>
- Didan, K. (2021). MODIS/Terra Vegetation Indices 16-Day L3 Global 1km SIN Grid V061 [Dataset]. <https://doi.org/10.5067/MODIS/MOD13A2.061>
- Farquharson, L. M., Mann, D. H., Grosse, G., Jones, B. M., & Romanovsky, V. (2016). Spatial distribution of thermokarst terrain in Arctic Alaska. *Geomorphology*, 273, 116–133. <https://doi.org/10.1016/j.geomorph.2016.08.007>
- Farquharson, L. M., Romanovsky, V. E., Cable, W. L., Walker, D., Kokelj, S., & Nicolisky, D. (2019). Climate change drives widespread and rapid thermokarst development in very cold permafrost in the Canadian high Arctic. *Geophysical Research Letters*, 46(12), 6681–6689. <https://doi.org/10.1029/2019gl082187>
- Fraser, R., Kokelj, S. V., Lantz, T. C., McFarlane-Winchester, M., Olthof, I., & Lacelle, D. (2018). Climate sensitivity of high arctic permafrost terrain demonstrated by widespread ice-wedge thermokarst on banks Island. *Remote Sensing*, 10(6), 954. <https://doi.org/10.3390/rs10060954>
- Frost, G., Christopherson, T., Jorgenson, M. T., Liljedahl, A. K., Macander, M. J., Walker, D. A., & Wells, A. F. (2018). Regional patterns and asynchronous onset of ice-wedge degradation since the mid-20th century in Arctic Alaska. *Remote Sensing*, 10(8), 1312. <https://doi.org/10.3390/rs10081312>
- Gilbert, G. K. (1909). The convexity of hillslopes. *The Journal of Geology*, 17(4), 344–350. <https://doi.org/10.1086/621620>
- Jones, B. M., Grosse, G., Arp, C. D., Miller, E., Liu, L., Hayes, D. J., & Larsen, C. F. (2015). Recent arctic tundra fire initiates widespread thermokarst development. *Scientific Reports*, 5(1), 15865. <https://doi.org/10.1038/srep15865>
- Jorgenson, M. T., Kanevskiy, M., Shur, Y., Moskalenko, N., Brown, D. R. N., Wickland, K., & Koch, J. (2015). Role of ground ice dynamics and ecological feedbacks in recent ice wedge degradation and stabilization. *Journal of Geophysical Research: Earth Surface*, 120(11), 2280–2297. <https://doi.org/10.1002/2015jf003602>
- Jorgenson, M. T., Kanevskiy, M. Z., Jorgenson, J. C., Liljedahl, A., Shur, Y., Epstein, H., et al. (2022). Rapid transformation of tundra ecosystems from ice-wedge degradation. *Global and Planetary Change*, 216, 103921. <https://doi.org/10.1016/j.gloplacha.2022.103921>
- Jorgenson, M. T., Shur, Y., & Pullman, E. R. (2006). Abrupt increase in permafrost degradation in Arctic Alaska. *Geophysical Research Letters*, 33(2), L02503. <https://doi.org/10.1029/2005GL024960>
- Kanevskiy, M., Shur, Y., Jorgenson, T., Brown, D. R., Moskalenko, N., Brown, J., et al. (2017). Degradation and stabilization of ice wedges: Implications for assessing risk of thermokarst in Northern Alaska. *Geomorphology*, 297, 20–42. <https://doi.org/10.1016/j.geomorph.2017.09.001>
- Kanevskiy, M., Shur, Y. L., Jorgenson, M. T., Ping, C.-L., Michaelson, G., Fortier, D., et al. (2013). Ground ice in the upper permafrost of the Beaufort Sea coast of Alaska. *Cold Regions Science and Technology*, 85, 56–70. <https://doi.org/10.1016/j.coldregions.2012.08.002>
- Krahenbul, P., & Koltun, V. (2011). Efficient inference in fully connected CRFS with Gaussian edge potentials. *Advances in Neural Information Processing Systems*, 24, 109–117.
- Lachenbruch, A. H. (1962). *Mechanics of thermal contraction cracks in permafrost*. Geological Society of America.
- Leffingwell, E. K. (1919). Ground-ice wedges: The dominant form of ground-ice on the north coast of Alaska. *The Journal of Geology*, 23(7), 635–654. <https://doi.org/10.1086/622281>
- Liljedahl, A. K., Boike, J., Daanen, R. P., Fedorov, A. N., Frost, G. V., Grosse, G., et al. (2016). Pan-arctic ice wedge degradation in warming permafrost and its influence on tundra hydrology. *Nature Geoscience*, 9(4), 312–318. <https://doi.org/10.1038/ngeo2674>
- Mackay, J. R. (1990). Some observations on the growth and deformation of epigenetic, syngenetic and anti-syngenetic ice wedges. *Permafrost and Periglacial Processes*, 1, 15–29. <https://doi.org/10.1002/ppp.3430010104>
- Mackay, J. R. (1995). Ice wedges on hillslopes and landform evolution in the late quaternary, Western Arctic coast, Canada. *Canadian Journal of Earth Sciences*, 32(8), 1093–1105. <https://doi.org/10.1139/e95-091>
- Mackay, J. R. (2000). Thermally induced movements in ice-wedge polygons, western Arctic coast: A long-term study. *Géographie Physique et Quaternaire*, 54(1), 41–68. <https://doi.org/10.7202/004846ar>
- Magnusson, R. I., Hamm, A., Karsanaev, S. V., Limpens, J., Kleijn, D., Frampton, A., & Heijmans, M. M. P. D. (2022). Extremely wet summer events enhance permafrost thaw for multiple years in Siberian tundra. *Nature Communications*, 13(1), 1556. <https://doi.org/10.1038/s41467-022-29248-x>
- McAfee, S. A., Walsh, J., & Rupp, T. S. (2013). Statistically downscaled projections of snow/rain partitioning for Alaska. *Hydrological Processes*, 28(12), 3930–3946. <https://doi.org/10.1002/hyp.9934>
- McKean, J. A., Dietrich, W. E., Finkel, R. C., Southon, J. R., & Caffee, M. W. (1993). Quantification of soil production and downslope creep rates from cosmogenic <sup>10</sup>Be accumulations on a hillslope profile. *Geology*, 21(4), 343–346. [https://doi.org/10.1130/0091-7613\(1993\)021<0343:qospad>2.3.co;2](https://doi.org/10.1130/0091-7613(1993)021<0343:qospad>2.3.co;2)
- Mekonnen, Z. A., Riley, W. J., Grant, R. F., & Romanovsky, V. E. (2021). Changes in precipitation and air temperature contribute comparably to permafrost degradation in a warmer climate. *Environmental Research Letters*, 16(2), 024008. <https://doi.org/10.1088/1748-9326/abc444>
- Minke, M., Donner, N., Karpov, N. S., de Klerk, P., & Joosten, H. (2007). Distribution, diversity, development and dynamics of polygon mires: Examples from northeast Yakutia (Siberia). *Peatlands International*, 1, 36–40.
- NASA Global Modeling and Assimilation Office. (2015). MERRA-2 2d, 1-hourly, instantaneous, single-level, assimilation, land surface forcings v5.12.4 [Dataset]. *Goddard Earth Sciences Data and Information Services Center (GES DISC)*. <https://doi.org/10.5067/RCMZA6TL70BG>
- Nitzbon, J., Langer, M., Martin, L. C. P., Westermann, S., von Deimling, T. S., & Boike, J. (2021). Effects of multi-scale heterogeneity on the simulated evolution of ice-rich permafrost lowlands under a warming climate. *The Cryosphere*, 15(3), 1399–1422. <https://doi.org/10.5194/tc-15-1399-2021>
- Nitzbon, J., Langer, M., Westermann, S., Martin, L., Aas, K. S., & Boike, J. (2019). Pathways of ice-wedge degradation in polygonal tundra under different hydrological conditions. *The Cryosphere*, 13(4), 1089–1123. <https://doi.org/10.5194/tc-13-1089-2019>
- Nitzbon, J., Westermann, S., Langer, M., Martin, L. C. P., Strauss, J., Laboor, S., & Boike, J. (2020). Fast response of cold ice-rich permafrost in northeast Siberia to a warming climate. *Nature Communications*, 11(1), 2201. <https://doi.org/10.1038/s41467-020-15725-8>
- Obu, J., Westermann, S., Bartsch, A., Bernikov, N., Christiansen, H. H., Dashtseren, A., et al. (2019). Northern hemisphere permafrost map based on ttop modelling for 2000–2016 at 1 square kilometer scale. *Earth-Science Reviews*, 193, 299–316. <https://doi.org/10.1016/j.earscirev.2019.04.023>
- Painter, S. L., Coon, E. T., Jan, A., & Jastrow, J. D. (2023). Drying of tundra landscapes will limit subsidence-induced acceleration of permafrost thaw. *Proceedings of the national academy of sciences* (Vol. 120(8), e2212171120), <https://doi.org/10.1073/pnas.2212171120>
- Poggio, L., de Sousa, L. M., Batjes, N. H., Heuvelink, G. B. M., Kempen, B., Ribeiro, E., & Rossiter, D. (2021). Soilgrids 2.0: Producing soil information for the globe with quantified spatial uncertainty. *Soils*, 7(1), 217–240. <https://doi.org/10.5194/soil-7-217-2021>

- Porter, C., Morin, P., Howat, I., Noh, M., Bates, B., Peterman, K., et al. (2018). Arctic DEM, v1 [Dataset]. *Harvard Dataverse*. <https://doi.org/10.7910/DVN/OHHUKH>
- Raynolds, M. K., Walker, D. A., Ambrosius, K. J., Brown, J., Everett, K. R., Kanevskiy, M., et al. (2014). Cumulative geoecological effects of 62 years of infrastructure and climate change in ice-rich permafrost landscapes, prudhoe bay oilfield, Alaska. *Global Change Biology*, 20(4), 1211–1224. <https://doi.org/10.1111/gcb.12500>
- Rettelbach, T., Langer, M., Nitze, I., Jones, B., Helm, V., Freytag, J. C., & Grosse, G. (2021). A quantitative graph-based approach to monitoring ice-wedge trough dynamics in polygonal permafrost landscapes. *Remote Sensing*, 13(16), 3098. <https://doi.org/10.3390/rs13163098>
- Rumpca, C. T., Abolt, C. J., Atchley, A. L., & Harp, D. R. (2024). A neural network for cloud masking in worldview satellite imagery [Software]. *Environmental System Science Data Infrastructure for a Virtual Ecosystem*. <https://doi.org/10.5440/1834771>
- Shur, Y., Hinkel, K. M., & Nelson, F. E. (2005). The transient layer: Implications for geocryology and climate-change science. *Permafrost and Periglacial Processes*, 16(1), 5–17. <https://doi.org/10.1002/ppp.518>
- Smith, N. D., Burke, E. J., Aas, K. S., Althuisen, I. H. J., Boike, J., Christiansen, C. T., & Chadburn, S. E. (2022). Explicitly modeling microtopography in permafrost landscapes in a land surface model (Jules vn5.4\_microtopography). *Geoscience Model Development*, 15, 3603–3639.
- Vercauteren, T., Pennec, X., Perchant, A., & Ayache, N. (2009). Diffeomorphic demons: Efficient non-parametric image registration. *NeuroImage*, 45(1), 61–72. <https://doi.org/10.1016/j.neuroimage.2008.10.040>